Coronal Seismology

Laurel Farris
New Mexico State University
laurel07@nmsu.edu

ABSTRACT

Coronal seismology involves the investigation of magnetohydrodynamic (MHD) waves and oscillatory phenomena that arise in the solar corona. Properties of the observed modes are largely dependent on their environment, and therefore can be used to extract atmospheric parameters that are otherwise difficult to observe. The general theory behind MHD phenomena is investigated here, along with the characteristics of different modes and the information that can be extracted from them. A few methods are applied to data from the *Atmospheric Imaging Assembly* (AIA) instrument on the *Solar Dynamics Observatory* (SDO).

Subject headings: Sun: corona-Sun: oscillations-Sun: seismology

1. Introduction

The solar corona is characterized by various types of structures, such as coronal loops, filaments, and bright points. These are formed by plasma flowing along magnetic field lines and emitting light primarily in the EUV. Disturbances on the sun can be seen in the form of oscillations or waves propagating through such structures, which act as waveguides. Such disturbances can be triggered by flares and coronal mass ejections (CMEs), or by continuous excitations from photospheric motions and global seismological modes, such as pressure modes, in the solar interior. The behavior of these waves can be described using the theory of magnetohydrodynamics (MHD). Different MHD modes have different characteristic speeds, which are related to other physical properites of the corona, such as magnetic field strength and density, which are difficult to measure directly (Verwichte et al. (2013)).

Here, the properties of MHD modes are investigated, along with literature from a variety of authors in the field. The basic concepts of MHD waves and oscillations are described in §2, and §3 covers several MHD modes in detail. A description of a research project and the results are presented in §5. Conclusions and future work are discussed in §6.

2. Basic MHD

2.1. Types of Modes

The relationship between MHD modes can be best understood by their relative phase speeds. A dispersion diagram is shown in figure 1, which plots the variation of phase velocity as a function of wavenumber for different modes. to the internal and external Alfvén and sound speeds. Each of these curves represents a solution to the dispersion relation, which is outside the scope of this paper. There are two primary characteristic speeds determined by the properties of the surrouding medium. The acoustic, or sound speed (C_s), is driven by thermal pressure of the gas, and is given by:

$$C_s = \sqrt{\frac{\gamma P}{\rho}} \tag{1}$$

In contrast, the Alfvén speed is magnetically driven, and is dependent upon the magnetic field strength. It is given by:

$$C_A = \frac{B}{\sqrt{4\pi\rho}} \tag{2}$$

In general, MHD waves are divided into two categories: Alfvén waves and magnetoacoustic waves. Magnetoacoustic waves can be *slow* or *fast*, depending on how the velocity of the wave compares to the local sound speed, C_s. Slow-mode magnetoacoustic waves have phase speeds roughly equal to C_s in the medium in which they reside, analogous to typical acoustic waves, or sound waves. Fast-mode magnetoacoustic waves have

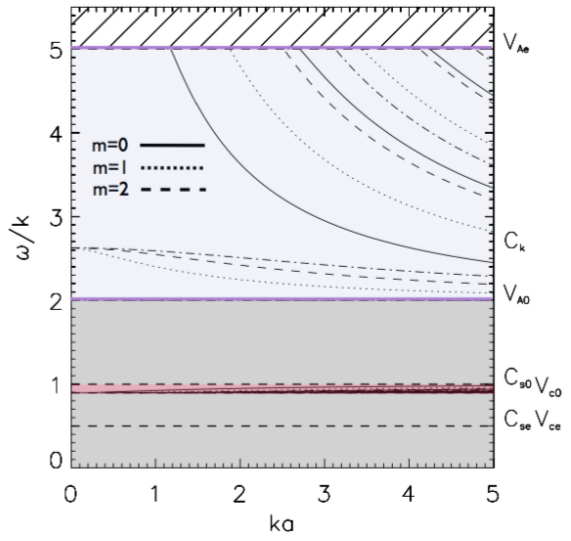

Fig. 1.— Dispersion diagram showing the variation in phase velocity as a function of wavenumber. The phase velocity is expressed as a factor of the internal sound speed, and the wavenumber is multiplied by the factor a to give it dimensionless units. Image credit: Nakariakov & Verwichte (2005)

phase speeds comparable to the Alfvén speed, or $\omega/k \approx V_A$ (Aschwanden et al. (1999)).

Each MHD mode is characterized based on a number of qualities, such as its wavelength, period, lifetime, speed, and whether it is propagating or standing, fast or slow, longitudinal or transverse, etc. The driving mechanisms that give rise to each mode can differ depending on these qualities and the environment in which the modes reside, and is one of the important MHD topics under investigation, along with the damping mechanism (Aschwanden et al. (1999)).

2.2. Equations and Models

MHD waves are often modeled with a straight, cylindrical flux tube embedded in a uniform magnetic field. The interior values of magnetic field strength (**B**), mass density (ρ), pressure (P), and temperature (T) are different from the exterior values.

2.3. Excitation and Damping Mechanisms

2.3.1. Resonant Absorption

If the frequency of a wave falls within one of two types of MHD continua (namely, the Alfvén or cusp continua), a resonance will occur. In the cylinder model, this location is a shell at radius r. In the Alfvén continuum, the Alfvén wave is the mode that is resonantly excited and dissipates in the corona. This is one of the processes thought to contribute to the heating of the corona. It involves the conversion from a collective mode to a local mode, at a timescale much shorter than that of the dissipative damping. To analyze this mathematically, equations of ideal MHD cannot be used because dissipation effects must be taken into account (Nakariakov & Verwichte (2005)).

2.3.2. Phase Mixing

Another effect associated with wave modes from MHD continua is called phase mixing, and is also a possible mechanism driving the heating of the solar corona.

2.4. Observation Techniques

Due to the lack of spatial resolution for the scales at which MHD oscillations occur, many are detected using time series analysis, where the periodic changes in intensity are analyzed as a function of time. As sufficient spatial resolution was developed, more observations of physical phenomena were made possible, such as the transverse displacement of coronal loops by kink oscillations (see § 3.1).

Density variations are usually observed as intensity variations, 180° out of phase. Oscillations are often observed in coronal loops as modes reflected back and forth between the loop footpoints, which are anchored in the photosphere and act as the wave nodes. For insufficient spatial resolution (or line-of-sight (LOS) angle), Doppler shifts can be extracted.

Often, it is the period of oscillation that is directly measured from observations. The general relationship between period and other wave parameters for the fundamental oscillating mode is given by:

$$P = \frac{\lambda}{C_{ph}} \tag{3}$$

where λ is the wavelength. For example, in a coronal loop of length ℓ, the wavelength is given by $\lambda = 2\ell$.

3. Types of MHD Modes

The behavior of MHD modes can vary based on whether they are fast or slow, stading or propagating, etc. These are discussed below, along with short literature reviews of work that has been done to observe, identify, and utilize these modes to extract physical coronal parameters.

3.1. Kink Oscillations

Kink oscillations are directly observed in coronal loops in extreme ultraviolet (EUV) wavelengths. They characterize the spacial oscillations that occur over the surface of the loop, perpendicular to the direction traversed by the length of the loop (Nakariakov & Verwichte (2005)). Kink oscillations generally are not accompanied by intensity variations; they displace the axis of the magnetic structure in which they propagate, but the cross-section of the waveguide remains roughly the same. Kink oscillations occur in the "long-wavelength regime", which is defined by the product of the wavenumber and the cross-section of the coronal loop being much less than 1 ($ka \ll 1$). In other words, the wavelength of the oscillation is much greater than the cross-section of the waveguide. The phase speed is just above the Alfvén speed within the loop, and the period of the oscillation is expected to be between $\sim$ 2 and 20 minutes (Aschwanden (2004)). Observations of kink oscillations are important to solar physics as the magnetic field strength can be derived from the period.

Due to a lack of sufficient instrumentation, spatial variations such as those caused by kink oscillations were not resolved until the launch of the *Transition Region And Coronal Explorer* (TRACE) spacecraft. Some of the first results from preliminary TRACE data were produced by Aschwanden et al. (1999) after investigating oscillations detected in coronal loops. Images in the 171 Å and 195 Å extreme ultraviolet (EUV) bandpasses revealed several coronal loops undergoing transverse oscillations triggered by a nearby class M4.6 solar flare that occurred in July of 1998.

To identify the type of mode, they first isolated the oscillating loop by creating *running difference* images to subtract out the static background features. They then measured the period of the oscillation by tracking the spatial displacement of the isolated loop through time. The use of different locations along the length of the loop was a significant diagnosis technique, as it allowed for the discrimination between standing oscillations and propagating waves, as long as at least half of the loop length was detectable for determining any evidence of a phase shift.

Aside from the detection and identification of the kink mode, these observations also explored the possible triggers of MHD oscillations, a phenomenon that is not yet well constrained. The similarity in period and phase of all five loops indicated a common triggering mechanism, most likely the nearby flare. As there was some physical distance between the flare site and the loops, the excitation must have been a disturbance generated by the flare that then traveled to the footpoints of the loops.

The observations had enough qualities characteristic of fast kink modes, including the spatial displacements characteristic of this asymmetrical mode, to identify these oscillations as kink modes. An average period of $T = 269 \pm 6$ seconds, or roughly 4.5 minutes, was obtained, which fit well with the theoretical period for kink oscillations. The absence of any phase shift along the length of the loops revealed that these were *standing waves*, with nodes located at the loop footpoints.

The ability to identify kink modes has great significance for solar physics due to a correlation between the oscillation period, P, and the magnetic field strength, B, of the loop:

$$P \propto \frac{L}{\sqrt{n}} B \tag{4}$$

where L is the loop length and n is the number density, both of which can be (roughly) estimated from known coronal conditions. Kink waves are *Alfvénic*; their phase speed is close to that of the internal Alfvén speed: $C_k \gtrsim V_A$

More recently, Pascoe et al. (2015) investigated the driving mechanism behind the production and damping of the kink mode. This was found to occur on rapid timescales for both standing and propagating kink modes, both of which are consistently found throughout the solar corona. How-

ever, the mechanism behind the rapid damping of these modes was unclear. The gravitational stratification of the atmosphere could have the effect in increasing the velocity amplitude, thus reducing the attenuation caused by mode-coupling.

They compared two possible functional forms of the damping profile of the driver: that of a Gaussian and an exponential form. The Gaussian was a potential form of the amplitude variation at a lower height (z), while the variation at higher z took the form of an exponential. While the noise level of the data was too high to distinguish between the two forms, the simulations followed the form of a Gaussian.

They also considered the effect of the spatial profile of the driver itself on the excitation and subsequent damping of the kink waves. Two different possibilities were explored here: the effect of a "highly structured" driver including only the exponential damping profile, which they found to be unrealistic, and the effects of small-scale (i.e. less than the size of the loop cross-section) of eddies and photospheric motions around the footpoints of the loops. These motions can excite kink modes along the length of the coronal loop, but not as efficiently as those produced by larger scale motions. These motions are what determine the properites of the observed modes. The observed damping of the kink mode was found to be a result of mode-coupling and subsequent energy transfer from the characteristic transverse motions of the kink mode, to azimuthal motions. The period observed by *CoMP* was centered around 5 minutes, fitting within the expected kink period of 2-20 minutes. The phase speed was around 0.6 Mm s^{-1}, leading to a calculated wavelength of about 180 Mm.

3.2. Sausage Oscillations

In contrast to kink oscillations, sausage oscillations do not displace the axis of the structure in which they reside. However, they do cause a periodic change in the cross-section of the waveguide, and hence are observable through changes in intensity (and therefore density, due to flux conservation). Sausage oscillations only exist shortward of the long wavelength cutoff, where the wavelength is comparable to the cross-section of the loop in which they oscillate. Therefore they can only exist in loops that are "sufficiently thick and dense" (Yuan et al. (2013)).

Lopin & Nagorny (2015) plotted the changes in intensity and cross-sectional area for sausage oscillations in photospheric pores extending up through the solar atmosphere. They used the general cylinder model for the pores, though it is more likely that the cross-sectional area of the waveguide increases with height as the temperature increases and density decreases. Sausage waves are characterized by a change in the cross-section, but no displacement of the loop axis. They occur on much shorter timescales than kink waves. The relationship between pore size and intensity can indicate

Morton et al. (2011) investigated oscillations associated with magnetic pores, which are essentially small sunspots with an upper limit of about 1700 km in diameter and consist of an umbra, but no penumbra. These features have high magnetic strength ($\sim$ 1700 G) in the photosphere and expand in diameter as the height above the photosphere increases into the chromosphere. As magnetic flux is always conserved, observing the size of these features in the upper layers of the atmosphere can reveal their size in the photosphere, which is not as easily observable. However, this requires knowledge of their magnetic strength in the atmosphere as well. These pores act as a waveguide (much like the way coronal loops act as a waveguide). Observations along the line of sight reveal periodic changes in intensity due to the change in cross-section characteristic to sausage modes. These two variations are 180° out of phase, as an increase of surface area corresponds to a decrease in density, and hence, a decrease in intensity. The observed period for These modes was about 30-450 seconds, and they were considered as a possible heating mechanism for the corona. However, some wavelengths are reflected at the transition regions, while other make it through, and the ones that do make it through are not abundant enough to heat the corona to the temperatures that are observed.

3.3. Acoustic Oscillations

Srivastava & Dwivedi (2010) used data from the *Extreme Ultraviolet (EUV) Imaging Spectrometer* (EIS) on board the *HINODE* spacecraft to derive periodicities of disturbances observed above bright points (BPs) in the corona. While the propagation

of magnetoacoustic waves can be observed in the solar atmosphere, they do not carry enough energy to physically propagate there (and thus were ruled out as a possible mechanism of heating the corona or accelerating the solar wind).

They used intensity oscillations of a few different ionization species to pinpoint the origin and progression of magnetoacoustic waves between bright points in the photosphere, through the transition regions, and up into the corona. The time series of intensity oscillations was converted into a power spectrum, and periodicities were extracted using wavelet analysis and periodograms (note here on what exactly these are?). The periods they derived ($\sim 263 \pm 80$ s for the He II 256.32 Å emission line and $\sim 241 \pm 60$ s for the Fe XII 195.12 Å emission line) were close to the 5-minute global oscillations of the sun.

The relatives periodicities of acoustic oscillations were recognized as important characteristics, and modeled by Roberts et al. (1984). They recognized magnetoacoustic oscillations as a useful way to determine other properties of the solar atmosphere.

3.4. Propagating Acoustic Waves

The MHD modes that have been discussed up to this point are considered *standing* modes: oscillations with nodes in a fixed position, such as the footpoints of coronal loops anchored in the photosphere, or the points at the photosphere and chromosphere where acoustic oscillations with frequencies less than the cutoff are trapped. In contrast, *propagating* waves have nodes that move with time (though two propagating waves traveling in opposite directions can have a net result of a single, standing oscillation; see Aschwanden (2004), ch. 8). Propagating acoustic waves have been observed in both closed loops (where the wave decays before it can reach the other footpoint and reflect back; see Roberts et al. (1984)) and open structures. Waves with propagations speed much lower than the local Alfvén speed, are categorized as slow magnetoacoustic waves. These waves travel along magnetic field lines at speeds roughly equal to the local sound speed.

The changes in intensity along the same location as these waves propagate in time are mapped side by side to give time-distance information. The period, wavelength, propagation speed, and amplitude can all be derived using this method. Since the local sound, C_s is related to temperature, T, as

$$c_s \propto \sqrt{T} \tag{5}$$

a difference in observed propagation speeds implies a changing temperature profile in the transverse direction across the loop (Nakariakov & Verwichte (2005)).

Propagating acoustic waves are generally observed as "propagating disturbances" awaiting further diagnoses of magnetoacoustic waves, whose amplitudes are rather weak, requiring careful, detailed data analysis to acquire good signal-to-noise (S/N).

One of the first studies to analyze simultaneous observations at different wavelengths was carried out by Robbrecht et al. (2001) using data from two different instruments: the Extreme ultraviolet Imaging Telescope (EIS) on the Solar and Heliospheric Observatory (SOHO) and the Transition Region And Coronal Explorer (TRACE). These wavelengths, along with their corresponding ions emitting at those wavelengths, the temperature, and other relevant quantities from the study are given in table 1. Both instruments observed AR

instrument	EIT	TRACE
ion	Fe XII	Fe IX
wavelength	195 Å	171 Å
cadence	15 s	25 s
temperature	1.6 MK	1 MK
sound speed	192 km s^{-1}	152 km s^{-1}
propagation speed	110 km s^{-1}	95 km s^{-1}

Table 1: Relevant quantities from Robbrecht et al. (2001)

8218, where the presence of "weak transient disturbances" were revealed, and later classified as slow, propagating magnetoacoustic waves, with speeds that varied between 65 and 150 km s^{-1}. The expression for the formal sound speed of the ambient region was given by

$$c_s = 152 \sqrt{T} \text{ m s}^{-1} \tag{6}$$

where T is in units of Kelvin. This was compared to the observed speed of the propagating wave, which was derived from the slope of the

"ridges" on each of the four time-distance plots. The propagation speed of each wave was slightly ($\sim$ same order of magnitude) lower than the local sound speed. This difference was due to the angle between the loop and the plane of the sky against which the observations were made. The amount of time for a disturbance to pass a particular point was determined to be $\sim$ 169 s from the TRACE data. As both observations targeted the same wave, the significance of the differing speeds for each observation indicated a temperature gradient in the loop itself, indicating either a bundle of loop threads that make up a single loop, or a number of concentric shells that make up a single loop.

Because of the low amplitude of slow magnetoacoustic waves, their speeds can be difficult to determine observationally. Many techniques have been developed to extract these speeds with higher signal-to-noise ratio. One such technique involves the resonant behavior of "surfing signals" revealed by quasi-periodic disturbances (Uritsky et al. (2013)) The method did not rely on a well-defined periodicity, which made it particularly useful for slow magnetoacoustic waves, as they tend to exhibit quasi-periodic characteristics. It also had the capability to extract both negative and positive velocities, i.e. waves traveling both up and down coronal loops.

Since the phase speed of slow magnetoacoustic waves is determined by the local sound speed where they are produced ($\propto \sqrt{T}$), the wave speeds along different loops with different temperatures were expected to vary, but the frequencies were expected to be the same for waves excited by the same mechanism.

To test their technique on this temperature dependence for propagation velocities, Uritsky et al. (2013) used about 6 hours of observational data from the Atmospheric Imaging Assembly (AIA) on the Solar Dynamics Observatory (SDO). The technique was applied to the lines at 131 Å, 171 Å, 193 Å, and 211 Å, over the active region (AR) NOAA AR 11082, which was free of sunspots and high-energy flares. Though the actual driving mechanism behind the observed disturbances was uncertain, they did find the same relationship between sound speed and temperature as expressed in equation 5. The observed propagations were travelling primarily in the upward direction away from the footpoint, at speeds of about 40 to 180 km s^{-1} and periodicities between 4 and 8 minutes over all four channels.

The lack of dependence on linearity or consistent periods, this could be useful method for analysis of mixed modes or damping waves. Additionally, this study confirmed the temperature-dependence of slow-mode velocities in non-flaring locations free of sunspots.

3.5. Propagating Fast Waves

MHD modes that are categorized as "fast" (magnetoacoustic?) propagate at $\sim$ 570-800 km s^{-1}. These types of waves were investigated by Asai et al. (2012) using observations of a type of fast propagating wave called a *Moreton*. These waves are typically triggered by energetic flares and CMEs, with lifetimes of about 10 minutes. They were described as the intersection of MHD fast waves shock-propagating between the chromosphere and corona, and are observed in Hα. While they are rarely observed, their counterparts can be seen in the corona in the form of EIT waves (named after the *EUV Imaging Telescope* on the *Solar and Heliospheric Observatory*).

Asai et al. (2012) presented the first simultaneous observations of both a Moreton wave in Hα images, obtained from the *Solar Magnetic Activity Research Telescope* (SMART), along with 193 Å images from AIA (FeXII, at a temperature T=$10^{6.1}$ K), and 195 Å and 304 Å images from the *STEREO* instrument. The so-called EIT waves are EUV waves named after the instrument that first detected them, the *EUV Imaging Telescope* (EIT) on the *Solar and Heliospheric Observatory* (SOHO).

The Moreton wave was triggered by a class-X6.9 flare from AR NOAA 11263 that occurred on August 9, 2011. It lasted for $\sim$ 6 minutes, with an average velocity of $\langle v \rangle = 760$ km s^{-1}. The EUV waves were thought to be the coronal counterparts of the Moreton wave, although the difference in velocity and propagation direction showed that this was not the case. The EIT wave propagated at a velocity of 200-400 km s^{-1} and lasted for about 45-60 minutes, while the Moreton wave propagated at a velocity of 500-1500 km s^{-1} and only lasted for 10 minutes. Moreover, Moreton waves are quasi-isotropic, while the EIT waves were observed to

propagate isotropically.

Also observed were a filament and a promiance (two separate structures) that were near the region where the flare ocurred. The waves that resulted from the flare passed by these two structures, causing them to oscillate, and thus provide a valuable observable for diagnoising the propgating disturbances. The velocity of the propagating coronal wave was derived to be ~ 800 km s^{-1} from observations of the prominance, and ~ 570 km s^{-1} from observations of the filament. These numbers provided the expected velocity range for the coronal waves, placing them in the category of fast-mode MHD waves.

Wave	velocity [km s^{-1}]
F1	760
F2b	730
F2f	620
S2b	?
F3b	550
S3b	340
F3f	580

Table 2: Waves observed by Asai et al. (2012)

Another investigation of propagating fast waves was carried out by Yuan et al. (2013). They observed intensity perturbations of "quasi-periodic propagating fast magnetoacoustic wave trains" associated with AR 11227. These wave trains appeared $\sim$ 110 Mm from the center of the flare, 2.2 minutes after the flare occurred. They were only visible in the AIA 171 Å bandpass, suggesting a location restricted to a certain height range above the photosphere. They derived an average velocity of 833 km s^{-1}, which is in the Alfvén range. Three wavetrains were observed, travelling one behind the other with different wavelengths (periods) and different (initial) phase speeds (although they all ended with a phase speed of about 600 km s^{-1}. Comparisons between these waves and the radio spectrum of the flare acquired from the *Nançay Radioheliograph (NRH)* revealed that each wave train was triggered by a burst of radio energy caused by the acceleration of non-thermal electrons above the magnetic reconnection site. The periods of such waves follow a characteristic "tadpole" pattern, where the period decreases at a fixed height, which is 150 Mm here.

These could possibly be the kink mode if the waveguide was in the form of a loop. These can only be identified if the observed loop segment has the correct line of sight with respect to the observer. A longer wavelength results in a faster speed, which then results in the dispersion of fast magnetoacoustic waves. The range in propagating phase speeds they derived was $v_{ph} = 735 - 845$ km s^{-1}, with a final speed (post-dispersion) of 600 km s^{-1}.

3.6. Torsional Modes

Torsional modes, or more commonly, *Alfvén* modes, are axisymmetric modes whose speed is determined primarily by magnetic pressure forces (see equation 2). They are transverse waves that are highly anisotropic (Goossens (2003)), with a *group* speed that travels strictly along magnetic field lines in response to a restoring force that acts to resist shear. The *phase* speed can be at an angle θ to the direction of the magnetic field $\vec{B}$:

$$V_A = \pm \frac{B}{\sqrt{4\pi\rho}} \cos\theta \tag{7}$$

The energy carried by this wave is contained in the group speed (Somov (2013)).

In the classic cylindrical model of a plasma structure, Alfvén waves undergo torsion (aka, twisting), in opposite directions on either end of the cylinder (Nakariakov & Verwichte (2005)).

The primary damping mechanism for Aflvén waves is resonant absorption, and is thought to be a possible cause for coronal heating. However, they are difficult to observe because, like the kink mode, they do not cause an intensity change, and additionally do not displace the structure through which they travel, so there is no visual indication that they are present.

Tian et al. (2012) derived the magnetic field strength and Alfvén velocity using coronal seismology, and compared them to other techniques to confirm that coronal seismology was in fact a reliable method to determine these parameters. For the direct techniques, the magnetic field was found using magnetic extrapolation, and the Alfvén velocity was found using spectroscopic observations of the Fe XII λ 195.12 line, where the Doppler shifts along the line-of-sight (LOS) in a coronal loop could be used to measure velocities. For the

seismological applications, the AIA 171 Å data was used.

They also took into account the situation of a non-zero density gradient and magnetic stratification, a more realistic consideration than the ideal case of a flux tube with constant density inside and zero density outside (the contrast between the two is one of the aforementioned difficult parameters to determine in the corona).

The phase speed of the loop oscillation was found to be between 2500 and 2600 km s^{-1}. This range fit the characteristic kink speed, given by

$$C_k \approx \sqrt{\frac{2}{1+\zeta^{-1}}} V_A \tag{8}$$

where ζ is the ratio of the internal loop density to the external density, ρ_i/ρ_e.

The results allowed for the conclusion that coronal seismology is a reliable method for deriving these coronal parameters.

They did note that oscillations do not necessarily indicate MHD waves, as these same oscillations can result from upflows of jets, which were found to be the dominate source of the oscillations seen around the loop footpoints. Toward the top of the loop, the observed oscillations were in fact found to be due to either kink or Alfvén waves They also noted that intensity changes can occur as a result of the loop itself begin in motion, transversing back and forth across the slit location, and cautioned that a phase difference between intensity and Doppler shift was not an immediate indication of density perturbation, and further analysis should be carried out.

Alfvén waves can be difficult to observe (or at least difficult to identify observed disturbances as Alfvén waves) since, like kink oscillations, they do not cause any periodic changes in intensity or density. It follows that determining the Alfvén speed is also difficult, depending on what parameters are directly observable.

Verwichte et al. (2013) tested the accuracy of the coronal seismology technique by using those methods to determine the Alfvén speed, and hence the magentic field strength, and comparing the results to those from more "direct" methods of determining magnetic field strength, namely, magnetic extrapolation and spectroscopy. An X-class flare triggered oscillations in two coronal loops in AR 1123 in 2011. The loops were observed in the AIA/SDO 171 Å bandpass as transverse oscillations with periods of $\sim$ 2-3 minutes. Using the expression for the fundamental standing mode ($P = 2\lambda/V_{ph}$), the observed period and loop length were used to calculate the phase velocity, which was around 2500 km s^{-1}. Due to the tranverse nature of the oscillations and the relatively short periods, these were identified as kink oscillations. Using the expression for the kink speed in the low plasma-β environment, along with the assumption of a uniform density and magnetic field along the length of the loop, setting the phase velocity equal to the kink speed and solving for the Alfvén speed gives

$$V_A = V_{ph}\sqrt{\frac{1+\rho_e/\rho_i}{2}} \tag{9}$$

The ratio between the external (ρ_e) and internal (ρ_i) densities is a difficult value to measure, and is one of the primary reasons that Alfvén speeds are so hard to constrain. Here they used the DEM inversion technique to derive the density based on the observed intensity, and the magnetic field strength was extrapolated from the three-dimensional model of the coronal loops, represented as potential fields. They concluded that the two methods produced results similar enough to consider coronal seismology a reliable method. Previous studies had produced magnetic field strengths up to three times higher than those calculated using coronal seismology, but here this was thought to be due to a lack of consideration of loop stratification, rather than assuming constant density and magnetic field strength along the length of the loop, which extends far enough into the corona to undergo an overall gravitational stratification.

4. Discussion

The observational techniques and relevant properties of each of the different kinds of MHD waves are summarized in table 1.

5. Research Project

As part of the general topic of coronal seismology, a small research project was carried out. Several of the observational and analytical methods

Type of wave	Timescales	Sizescales	Observational techniques
Kink Oscillations	short	short	something
Sausage Oscillations	short	short	something
Acoustic Oscillations	x	x	x
Propagating	x	x	x

employed in the literature were emulated for this project, in addition to a cross-correlation analysis.

5.1. Data

An hour of data from AIA/*SDO* at 193 Å was examined for possible wave activity or notable disturbances. Each image in the time series was separated by 12 seconds, and taken during July of 2012. The first image in the series is shown in figure 2. The image clearly shows an active region

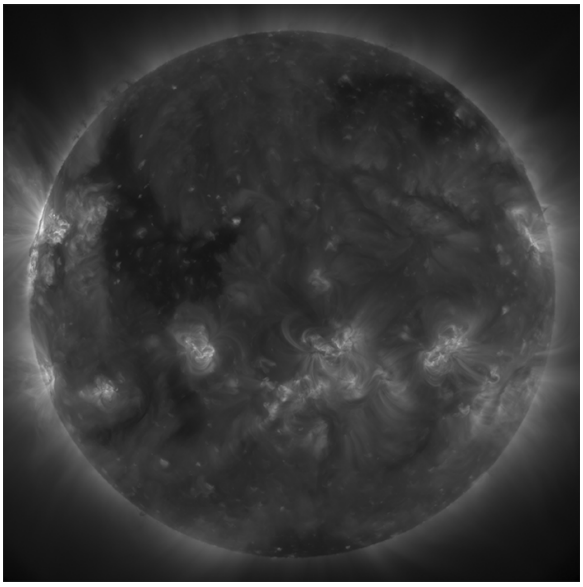

Fig. 2.— First image in the time series from AIA/*SDO*.

in the lower right region and a coronal hole in the upper left, with areas of quiet sun in between.

5.2. Lightcurves

To determine if there was a possible relationship between the size of the bright point and the intensity, the time variation of both quantities were plotted as shown in figure 3. There appears to be a possible correlation between the two, but further analysis is required, such as a fourier transform.

5.3. Cross-correlation

To check for variation or disturbances in the horizontal direction, i.e. outward from the center of the bright point in the radial direction, a cross-correlation was run between a single pixel located roughly in the center of the bright point, and every other pixel in the image shown in figure **??**.

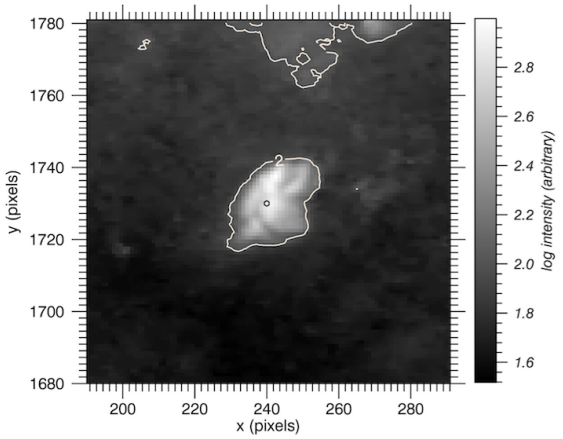

Fig. 4.— Image of the single bright point analyzed for this research. The contours outline the estimated size of the bright point using an intensity cutoff. The areas in the upper region of the image were also above the intensity threshold used to determine the size of the bright point, and hence are also outlined. The circle in the center indicates the location of the pixel that was correlated with every other pixel in the image.

6. Conclusion

The data set examined here requires further analysis, such as applying a Fourier Transform and finding exact locations for high correlation values. Data from the *Helioseismic and Magnetic Imager* (HMI) on *SDO* might be worth examining to see if a counterpart to the bright points can be seen in the photosphere. These techniques could be applied to the active region in the same data set,

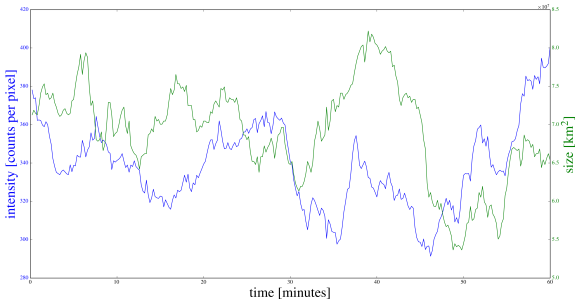

Fig. 3.— Size and intensity (counts per pixel) of the bright point as functions of time throughout the entire data series.

Fig. 5.— FIG. 2 (*a*) Image illustrating the maximum correlation value of each pixel with the central pixel; (*b*) Image of the timelag corresponding to the maximum correlation value of each pixel in *a*.

assuming they produce reliable results from the "cleaner" data in the coronal hole.

REFERENCES

Asai, A., Ishii, T. T., Isobe, H., et al. 2012, ApJ, 745, L18

Aschwanden, M. 2004, Physics of the Solar Corona: An Introduction

Aschwanden, M. J., Fletcher, L., Schrijver, C. J., & Alexander, D. 1999, The Astrophysical Journal, 520, 880

Goossens, M. 2003, An Introduction to Plasma Astrophysics and Magnetohydrodynamics, Vol. 294 (P.O. Box 17, 3300 AA Dordrecht, The Netherlands: Kluwer Academic Publishers)

Lopin, I., & Nagorny, I. 2015, ApJ, 810, 87

Morton, R. J., Erdélyi, R., Jess, D. B., & Mathioudakis, M. 2011, ApJ, 729, L18

Nakariakov, V. M., & Verwichte, E. 2005, Living Rev. Solar Phys.

Pascoe, D. J., Wright, A. N., De Moortel, I., & Hood, A. W. 2015, A&A, 578, A99

Robbrecht, E., Verwichte, E., Berghmans, D., et al. 2001, A&A, 370, 591

Roberts, B., Edwin, P. M., & Benz, A. O. 1984, ApJ, 279, 857

Somov, B. V. 2013, Plasma Astrophysics, Part I: Fundamentals and Practice, 2nd edn.

Srivastava, A. K., & Dwivedi, B. N. 2010, MNRAS, 405, 2317

Tian, H., McIntosh, S. W., Wang, T., et al. 2012, ApJ, 759, 144

Uritsky, V. M., Davila, J. M., Viall, N. M., & Ofman, L. 2013, ApJ, 778, 26

Verwichte, E., Van Doorsselaere, T., Foullon, C., & White, R. S. 2013, ApJ, 767, 16

Yuan, D., Shen, Y., Liu, Y., et al. 2013, A&A, 554, A144

This 2-column preprint was prepared with the AAS LaTeX macros v5.2.